J Physiol 587.5 (2009) pp 953–963

RAPID REPORT

Consequences of axon guidance defects on the development of retinotopic receptive fields in the mouse colliculus

Anand R. Chandrasekaran[1,2], Yas Furuta[3] and Michael C. Crair[1,4]

[1] *Graduate Program in Neuroscience, Baylor College of Medicine, Houston, TX 77030, USA*
[2] *Department of Bioengineering, Stanford University, Stanford, CA 94305, USA*
[3] *University of Texas M.D. Anderson Cancer Center, Houston, TX 77030, USA*
[4] *Department of Neurobiology, Yale University School of Medicine, New Haven, CT 06520, USA*

Gradients of molecular factors pattern the developing retina and superior colliculus (SC) and guide retinal ganglion cell (RGC) axons to their appropriate central target perinatally. During and subsequent to this period, spontaneous waves of action potentials sweep across the retina, providing an instructive topographic signal based on the correlations of firing patterns of neighbouring RGCs. How these activity-independent and activity-dependent factors interact during retinotopic map formation remains unclear. A typical phenotype of mutant mice lacking genes for one or more RGC axon guidance molecules is the presence of topographically inappropriate projections or 'ectopic spots'. Here, we examine mice that lack functional bone morphogenetic protein receptors (BMPRs) in the retina. Retinal BMP controls the graded expression of RGC axon guidance molecules, resulting in some dorsal RGCs projecting ectopically to locations in the SC that normally receive input from ventral retina. We examine the consequences of this anatomical phenotype *in vivo* by studying the receptive field (RF) properties of neurons in the superficial SC. We observe a mixture of physiological phenotypes in BMPR mutant mice; notably we find some neurons with ectopic RFs displaced in elevation, corresponding to the observed anatomical defect. However, in a result not necessarily congruent with the presence of focal ectopic projections, some neurons have split, enlarged and patchy/distorted RFs. These results are consistent with the effects of spontaneous retinal waves acting upon a disrupted molecular template, and they place significant limits on the form of an activity-dependent learning rule for the development of retinocollicular projections.

(Received 5 August 2008; accepted after revision 16 January 2009; first published online 19 January 2009)
Corresponding author M. C. Crair: Department of Neurobiology, Yale University School of Medicine, 333 Cedar Street, SHM C303, PO Box 208001, New Haven, CT 06520-8001, USA. Email: michael.crair@yale.edu

The brain represents the sensory periphery in a manner that preserves the spatial relationships between neighbouring sensory receptors. One such map of the visual world appears in the superficial layers of the superior colliculus (SC), which in the mouse is the primary target of retinal ganglion cell (RGC) afferents. In this retinotopic map, the dorsal–ventral (DV) axis of the retina maps along the lateral–medial (LM) extent of the SC, and the nasal–temporal axis maps along the anterior–posterior extent of the SC.

There are two major sources of topographic instruction in the development of retinotopic maps (for reviews see McLaughlin & O'Leary, 2005; O'Leary & McLaughlin, 2005; Torborg & Feller, 2005). The first is provided by gradients of axon guidance molecules that pattern the retina and the SC and act to direct RGC afferents to their proper targets. The second comes from the spatiotemporal properties of spontaneous retinal activity that occurs prior to eye opening. These retinal waves cause the coincident firing of nearby RGCs, which allow a Hebbian-like mechanism to strengthen or weaken nascent synapses appropriately to refine the retinotopic map (Hebb, 1949; Torborg & Feller, 2005; Shah & Crair, 2008). Both of these topographic instruction mechanisms are thought to act together to yield the final map, though their relative importance and interaction is difficult to ascertain.

To further study this issue, we used a line of bone morphogenic protein receptor (BMPR) mutant mice, which have an impaired pattern of retinocollicular

DOI: 10.1113/jphysiol.2008.160952

projections due to a disruption in the molecular regulation of DV patterning in the retina (Plas *et al.* 2008). We examined the emergence of SC neuron receptive fields in the BMPR mutant mice, which allows us to determine how activity-dependent instructive signals provided by spontaneous retinal waves interact with the molecular targeting of RGC axon projections to the SC.

Methods

Animals

Animals with null and conditional mutant alleles of the *Bmpr1a* gene (*Bmpr1a*$^{-}$ mice, Mishina *et al.* 1995; *Bmpr1a*^{fx} mice, Mishina *et al.* 2002) were used to generate mice that had a disrupted *Bmpr1a* gene in the retina using the *Six3Cre* transgene (Furuta *et al.* 2000). Cre-mediated recombination in *Six3Cre* transgenics is limited to the retina and ventral forebrain and begins at about E9.5 (Furuta *et al.* 2000). The conditional *Bmpr1a* allele results in a null allele upon Cre-mediated recombination (Bartlett *et al.* 2002). A combination of the null allele and conditional allele, mice trans-heterozygotes for these alleles (referred to as *Bmpr1a*$^{-/fx}$) and thus hemizygous for the *Bmpr1a* locus prior to Cre-mediated recombination, were used to conditionally disrupt the *Bmpr1a* gene. A null allele of *Bmpr1b* (*Bmpr1b*$^{-}$, Yi *et al.* 2000) was then introduced into the conditional *Bmpr1a* background. Animals lacking *Bmpr1a* and one copy of *Bmpr1b* (*Bmpr1a*$^{-/fx}$;*Bmpr1b*$^{+/-}$;*Cre*) are referred to in the text as BMPR mutant mice, while the controls were either *Bmpr1a*$^{+/fx}$;*Bmpr1b*$^{+/+}$;*Cre* or *Bmpr1a*$^{+/fx}$;*Bmpr1b*$^{+/-}$;*Cre* mice (Murali *et al.* 2005). BMPR mutant mice have no known morphological or physiological defects in retinal structure or function (Murali *et al.* 2005). Animals were treated in compliance with the Institutional Animal Care and Use Committee, US Department of Health and Human Services and Institution guidelines.

In vivo physiology

Adult mice were anaesthetized using urethane (1.0 g kg^{-1} I.P.) and injected with atropine (5 mg kg^{-1}) and dexamethasone (0.2 mg per mouse) as described previously (Chandrasekaran *et al.* 2005, 2007). Mice were then placed in a stereotaxic apparatus and their temperature and heart rate were monitored throughout the experiment. Anaesthetic was supplemented by 0.5–1% isoflurane in a mixture of oxygen and nitrous oxide (3 : 2). A craniotomy ($\sim$4 mm^2) was performed to expose the cortex overlying the colliculus and a tungsten microelectrode (0.5–5 M; FHC, Inc., Bowdoinham, ME, USA) was lowered into the SC using a hydraulic micromanipulator (David Kopf instruments). The responses obtained were amplified, filtered ($\times$10 000; 0.3–5 kHz; A-M Systems, Sequim, WA, USA) and digitized (25 kHz; National Instruments, Austin, TX, USA). Stimuli were presented using the Psychophysics Toolbox (Brainard, 1997; Pelli, 1997), and data acquisition was controlled by software written in MATLAB (The Mathworks Inc., Natick, MA, USA).

Receptive field reconstruction and analysis

Receptive fields (RFs) were reconstructed using previously published protocols (Chandrasekaran *et al.* 2007). Briefly, small (4–10 deg) square light stimuli were presented for 300 ms (7–12 cd m^{-2}) on a dim background (0.5–1 cd m^{-2}) with 900 ms between stimuli. Spatially overlapping stimuli were presented in pseudo-random order to form a grid in visual space and the RFs of cells were reconstructed from the averaged response to the stimuli. Background (spontaneous) visual activity was ascertained with interleaved blank stimuli. Spike waveforms were analysed offline to isolate single neurons from the recorded multiunit activity. Only cases with clear separation of voltage waveforms by visual inspection were considered well isolated. The RF was then fitted with an elliptical 2-D Gaussian function (Tavazoie & Reid, 2000; Chandrasekaran *et al.* 2005, 2007). The parameters extracted from the fitted Gaussian determined the location of the centre of the RF, the area, peak response, volume and elongation bias, if any (Chandrasekaran *et al.* 2005, 2007). A plot of the log of the Peak Response *vs.* the log of the Area was fitted with a straight line of slope -1 to determine if response homeostasis was maintained (Chandrasekaran *et al.* 2007).

Determination of electrode locations

To determine the location of the electrode on the surface of the SC, electrodes were coated with DiI between recordings and advanced systematically to new locations. At the end of the session, the animal was killed with an overdose of anaesthetic, and the brain removed and transferred to 1xPBS. Digital images were obtained of the surface of the SC after peeling off the cortex. The location of each electrode position was ascertained by the fluorescent trace left at the electrode entry location to the SC. Recordings from electrode locations with smeared or non-determinable traces were discarded.

Analysis of topography

Drager and Hubel generated an interpolated map of visual space for neurons in the superficial superior colliculus by hand-mapping the receptive fields of neurons sampled in a regular grid across the surface of the SC (referred to in this manuscript as the 'Drager

map'; Fig. 2*B*; Drager & Hubel, 1976). We used this map as a template to test for topographic accuracy of neurons in BMPR mutant and control mice. Receptive field locations and recording locations from DiI-coated electrodes for individual neurons were ascertained by mapping the responses to spots of light as described above. The locations of each electrode were parameterized by normalizing each colliculus to a square. The normalized electrode locations were then used to obtain an expected topographic location in visual space from the digitally re-sampled and similarly normalized Drager map. Errors in both azimuth and elevation (ΔAzimuth, ΔElevation) were quantified as the expected RF azimuth or elevation (from the Drager map) less the actual RF azimuth or elevation. Thus, positive values for ΔElevation correspond to RF locations that have a lower elevation than expected. For displaying the topographic accuracy of all cells obtained in a single animal, a colour-interpolated Drager map was constructed for each axis, azimuth and elevation, using filled contour plots and a customized colourmap.

Results

Receptive fields and response homeostasis in BMPR mutant mice

BMPR mutant mice have RGC axon guidance and branching defects that result in the formation of normal target zones as well as 'ectopic spots' or target zones at inappropriate locations in the superior colliculus (Murali *et al.* 2005; Plas *et al.* 2008). These ectopic spots are typical of mice with mutations in factors that regulate retinal ganglion cell axon guidance or branching, such as mice with mutations in the family of Eph/ephrin signalling molecules (for review, see McLaughlin & O'Leary, 2005). We examined the physiological consequences of ectopic projections in the map of visual space in the superior colliculus of BMPR mutant mice. Receptive fields of isolated neurons were obtained using *in vivo* single unit recording techniques in control and BMPR mutant mice blind to the genotype. Fifty-nine out of 81 recording locations had isolatable units from six control mice; 81/109 from eight BMPR mutants at 6–13 locations (neurons) in each mouse. RFs were fitted with a 2-D Gaussian following published methods (Chandrasekaran *et al.* 2005). Fits were comparable in control and BMPR mutant mice (mean Pearson's regression coefficient (r^2) of 0.78 ± 0.03 for 59 control neurons and 0.71 ± 0.04 for 81 BMPR mutant neurons, $P = 0.2$). RFs of neurons well fitted by the 2-D Gaussian ($r^2 > 0.5$ for 53/59 control cells and 74/81 BMPR mutants, including six mutant cells fitted by a double Gaussian) had parameters corresponding to the size, shape and location of the RF extracted (Chandrasekaran *et al.* 2005, 2007).

In control mice, RFs were typically circularly symmetrical or slightly elongated along the azimuth (paired comparison between azimuth and elevation: $P < 0.05$; see Chandrasekaran *et al.* 2005). In BMPR mutant mice, RFs were more varied in size and shape, occasionally even splitting into two circumscribed response fields, and there was no tendency for RF elongation along the azimuth (paired *t* test, $P = 0.13$). In the mouse SC, neurons with large RFs tend to have a smaller peak response so that the integrated total response is conserved on a cell-by-cell basis (Fig. 1*D*, and Chandrasekaran *et al.* 2007). This 'response homeostasis' is maintained in BMPR mutant mice, despite the larger variation in RF area and peak response (Fig. 1*E*, *F* and *G*; *t* test for similar mean values: $P > 0.05$ for RF area, peak response and total response; Levene test for equal variance: $P < 0.05$ for RF area and peak response between control and mutant mice. $P = 0.59$ for integrated total response between control and mutant mice). A plot of RF peak response *vs.* RF area in the log domain is well fitted by a line of slope -1 for BMPR mutant mice neurons (Fig. 1*D*; $n = 74$; $r^2 = 0.7$) and for control neurons ($n = 53$; $r^2 = 0.67$), consistent with the maintenance of total integrated response in both control and mutant mice.

Topographic errors in BMPR mutant mice

Anatomical targeting errors in BMPR mutant mice typically involve the misprojection of ventral RGC axons into ectopic spots in dorsal RGC target territory in the SC, consistent with the role of BMPs in acting as dorsalizing factors in the developing retina (Fig. 2*A* and *B*; Murali *et al.* 2005; Plas *et al.* 2008). Receptive fields in BMPR mutant mice reflect these targeting errors, so that we occasionally (38/315) observed pairs of recordings from disparate locations in the SC that had overlapping RFs (centres within 5 deg). This was rarely (2/223) observed in neurons recorded from control mice. For example, in Fig. 2*B* the RF centres of neurons from two distinct electrode locations in the SC of a BMPR mutant mouse overlap in visual space. The RF centres for these locations in the SC (according to the interpolated Drager map, see Methods) of a control mouse should be from parts of visual space with a higher elevation. This suggests that two different locations in the SC of BMPR mutant mice can receive input from the same region of the retina through 'ectopic' or misprojecting axons that should have terminated in a more lateral location of the SC.

We normalized our collicular images and the Drager map to a unit square for qualitative and quantitative comparisons of RF topographic error (see Methods). The recordings from control and mutant mice were overlaid on this map to visualize the topographic accuracy of RFs (Fig. 3). At the electrode location of each neuron, the location of the RF centre in either horizontal (azimuth) or

vertical (elevation) visual space is depicted using the same colour scale as the Drager map. In the control example shown, 13 recordings were obtained from one control mouse. Qualitatively, the topography of control mice with receptive fields determined by computer-controlled stimuli matches the Drager map well. In contrast, RF centres of 12 neurons from a BMPR mutant mouse show the occurrence of highly displaced (2/13 cells with >15 deg ΔAzimuth; 7/13 cells with >15 deg ΔElevation) locations compared to what was expected based on the Drager map.

The occurrence of receptive fields in the BMPR mutant mice with a positive shift in elevation (ΔElevation >0) is consistent with what is expected from the anatomical phenotype (Plas *et al.* 2008). We analysed the topographic error of the entire population of cells for which the RF location could be obtained from a single Gaussian fit (Fig. 3*B*; 53/53 control cells and 68/74 BMPR mutant cells). The topographic error of control cells is tightly clustered close to zero in both azimuth and elevation (mean ΔAzimuth, 1.5 ± 4.9 deg; mean ΔElevation, 0.6 ± 5.7 deg; error is in standard deviation). This illustrates that, despite the differences in method, the Drager map gives us values comparable with our control data, and can be used as an independent template to compare both control and mutant RF data. In contrast, the BMPR mutants have a dramatic shift in topographic error (ΔAzimuth, 3.0 ± 14.5 deg; $P = 0.5$

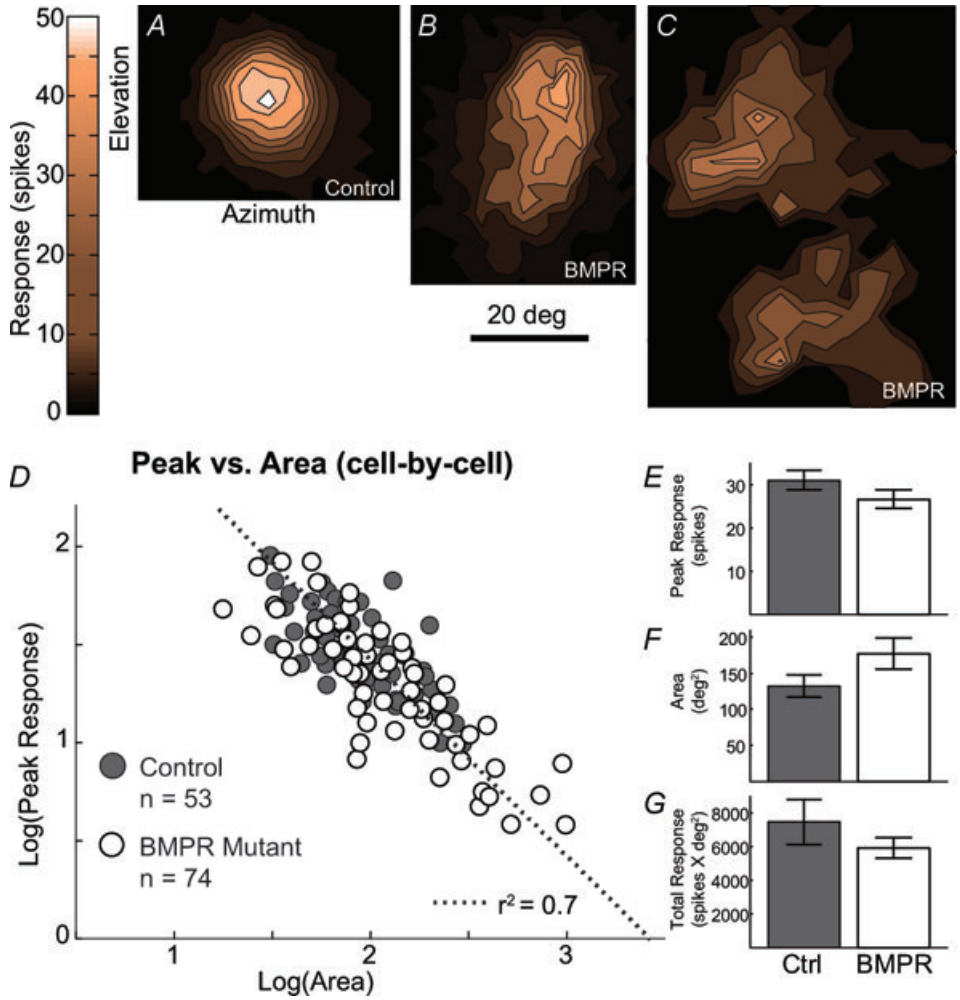

Figure 1. Abnormal RF shapes in BMPR mutants still obey response homeostasis
A, *B* and *C*, example RFs in control (*A*) and BMPR mutant (*B* and *C*) mice. *D*, log–log plot of RF Peak Response *vs.* RF Area in all neurons from both littermate controls and BMPR mutant mice are well fitted ($r^2 = 0.7$) by a line of slope –1, demonstrating that the changes in RF shape do not prevent neurons in the SC from maintaining response homeostasis. *E*, *F* and *G*, summary histograms of average RF Peak Response, Area and Total Response in the control (grey columns) and BMPR (white columns) mutant mice. There is no significant difference among the mean values of the three parameters. However, there is a significant difference between the variance for RF Area and Peak Response (Levene test: $P < 0.05$).

compared to control; ΔElevation, 19 ± 20 deg; $P \ll 0.01$ compared to control; *t* test for significant difference in mean; error is standard deviation). The difference in mean for the error in elevation is indicative of a strong ventral (retinal) shift in dorsal–ventral retinal topography, while the lack of a difference in the mean for error in azimuth shows no clear bias, but greater scatter than control mice in nasal–temporal error as well (Levene test for equal variance: $P \ll 0.01$ for nasal–temporal as well as dorsal–ventral error between control and mutant mice). Using 10 deg bins for values of ΔElevation, a regression line was fitted to the corresponding standard deviation of ΔAzimuth for BMPR mutant cells. This has a good fit ($r^2 = 0.51$) with a positive slope (0.21) indicating that the scatter in azimuth increases with increases in the scatter in elevation, suggesting that RFs that are ectopic in elevation (vertical visual space) are more likely to be ectopic in azimuth (horizontal visual space) as well.

Altered receptive fields in BMPR mutants

The salient physiological phenotype of the BMPR mutant mice is the presence of ectopic RFs (Fig. 4*B*; control 2/53; BMPR 18/74). These are RFs that deviate more than 15 deg from the predicted RF for that electrode location. In addition, receptive fields in BMPR mutants show an abnormal distribution of shapes that are not typically present in control mice. In particular, there is a high incidence of RFs that are elongated (defined as cells with a projection ratio > 1.25; see Chandrasekaran *et al.* 2005) vertically along elevation (Fig. 4*A* and *B*; Control 1/53; BMPR 13/74), which is consistent with a dorsal–ventral retinal ganglion cell targeting phenotype in the BMPR mutant mice. In contrast, we seldom observed RFs that were elongated horizontally along the azimuth (Fig. 4*B*; Control 6/53; BMPR 3/74). While these results are not unexpected, there is also a higher incidence of abnormally large RFs (>20 deg diameter) in BMPR mutants (Fig. 4*A* and *B*; Control 3/53; BMPR 12/74) and split (double Gaussian fit) RFs (Fig. 4*A* and *B*; Control 0/53; BMPR 6/74). These unusual RF shapes are not an obvious consequence of the anatomical defects observed in the BMPR mice.

Discussion

Ectopic spots lead to ectopic receptive fields

Anatomical studies of topographic mutants have yielded valuable information about the mechanisms responsible for mapping the retina onto its central targets. However, these anatomical studies tell us nothing about the functional consequences of misprojections, or whether 'ectopic axons' generate functional responses at all. We have demonstrated what happens to the receptive fields of individual neurons in a mutant with ectopic RGC projections. We provide evidence that the physiological map in the BMPR mutant, which has axon guidance defects along the dorsal–ventral axis (Plas *et al.* 2008), shows commensurate topographic disruption at the level of individual receptive fields.

BMPR mutants have pre-target-sorting errors, with dorsal RGC axons entering at the wrong location along the medial–lateral axis of the SC, resulting in a high proportion of dorsal axons projecting to inappropriate medial locations in the SC (Plas *et al.* 2008). The functional result, as evident from the topographic error analysis (Fig. 3), is a preponderance of inappropriate RF locations at lower elevations, corresponding to dorsal RGC axon misprojections to the medial colliculus. In addition to errors in RF elevation, we also found large errors in RF azimuth in the BMPR mutants. This error appears to have no bias towards either nasal or temporal directions, and its magnitude can be as large as the errors in elevation. There are several possible reasons for these large errors in azimuth. First, the ectopically targeted axons must compete with normally targeted axons for the same region in the SC landscape, resulting in a proportion of ectopic axons forced to branch in regions more anterior or posterior to the intended target location causing greater scatter in RF azimuth. It is also of note that the variance in azimuth error increases as the elevation error increases, suggesting that it is more likely that the ectopic axons lose the competition with normally targeted, appropriate axons. An alternative explanation is that cross-reactivity between the A and B families of ephrins might cause a disruption in targeting along both axes (Himanen *et al.* 2004). Finally, it is also possible that BMP directly affects both the dorsal–ventral and nasal–temporal fate in the developing retina.

Ectopic receptive fields provide clues to the nature of activity-dependent learning rules

Spontaneous retinal waves provide information about the relative positions of RGCs that is theoretically sufficient to refine retinotopy (Butts & Rokhsar, 2001). The retinotopic information provided by retinal waves is on a long time scale, utilizing timing differences from 100 ms up to 2 s. This suggests that bursts of action potentials (rather than single spikes) are the unit of information during development (Butts & Rokhsar, 2001). We previously demonstrated anatomically that the existence of ectopic spots required patterned retinal activity, otherwise misprojecting axons formed diffuse termination zones in the SC (Chandrasekaran *et al.* 2005). In the current study our physiological observations of split and patchy receptive fields in the BMPR mutants is not simply predicted by molecular guidance defects. However,

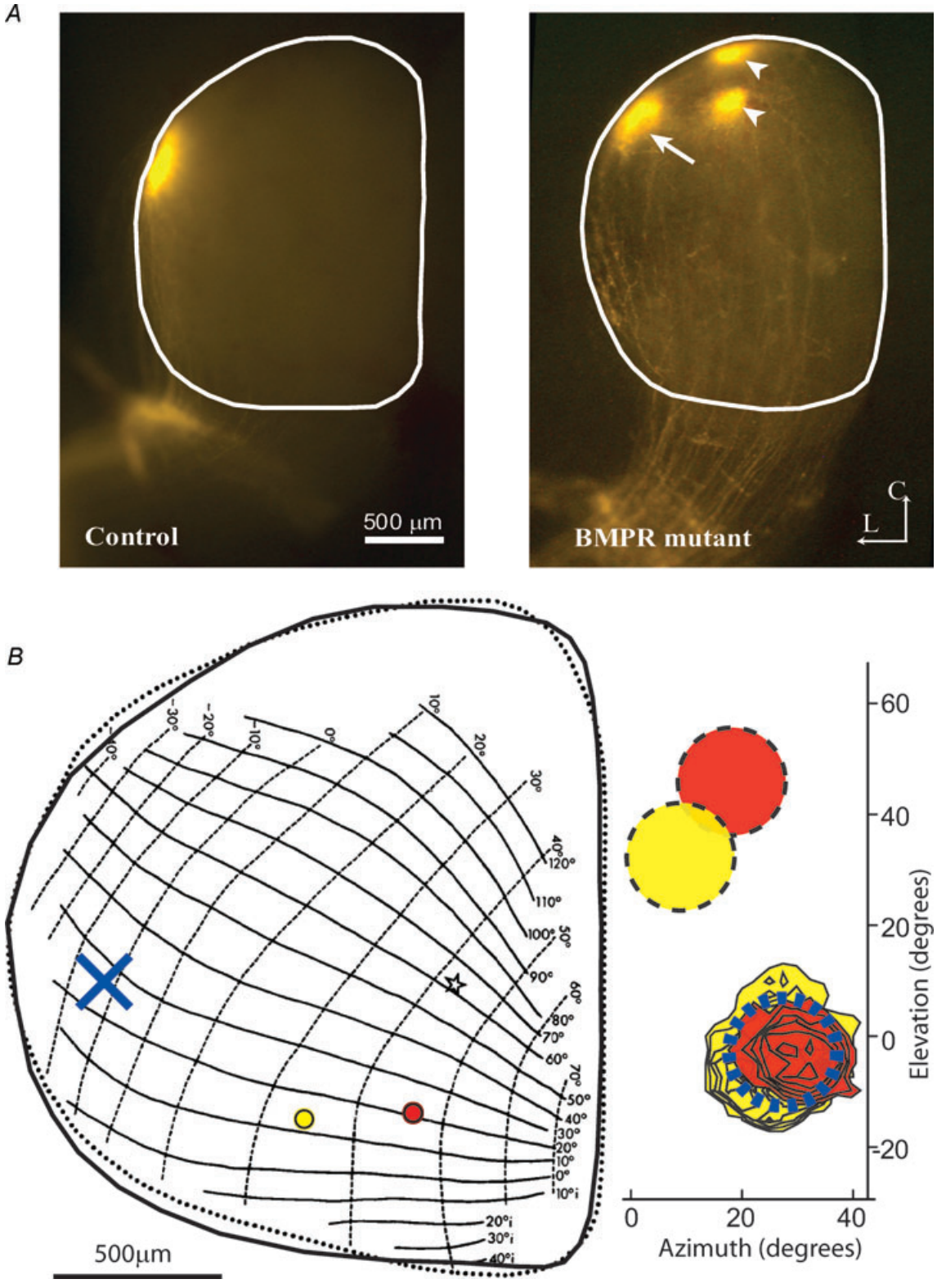

Figure 2. Ventralization of retinal axons in BMPR mutant mice
A, focal dorsal retinal injection in control animal results in a focal termination zone at the lateral edge of the colliculus (left). A similar focal injection in a BMPR mutant mouse (right) results in a normal target zone in lateral colliculus (arrow) as well as 2 additional ectopic target zones shifted medially (arrowheads). The SC is outlined in white. L is lateral, C is caudal. *B*, Drager's map of visual space (left, from Drager & Hubel, 1976) in the SC overlaid with an outline (continuous line) of the SC from an example BMPR mutant mouse. Indicated in red and yellow

we can explain the unusual patchy and split RFs by considering the effect of Hebbian learning rules on a disrupted molecular template. In control mice, a burst timing-dependent learning rule will stabilize coactive inputs from temporally synchronized neighbouring ganglions cells, leading to a high density cluster of axons in the SC from the appropriate location in the retina (Fig. 4, dark blue). In BMPR mutant mice, the initial guidance of RGC axons is impaired, resulting in regions of high axon density originating from inappropriate locations in the retina. When the magnitude of this targeting error is small, axons from nearby regions in the retina that are neither coactive nor directly competing against each other will innervate a single collicular cell. Synapses from both locations can survive, resulting in RFs that are elongated along the vertical (elevation) axis (Fig. 4, yellow). In control mice, there is a small tendency for RFs to be elongated along the horizontal (azimuth) axis, and this horizontal elongation is dramatically enhanced in retinal wave ($\beta2^{-/-}$) mutants (Chandrasekaran *et al.* 2005). The difference between control and BMPR mutant mice is consistent with a preferential role for molecular guidance factors to regulate DV topography, and retinal wave-based activity-dependent factors to preferentially refine nasal–temporal topography (Chandrasekaran *et al.* 2005; Cang *et al.* 2008).

As the magnitude of the targeting error increases in BMPR mutant mice, a cell in the SC is confronted with a choice between RGC axons from the appropriate region as well as an ectopic region of the retina. In this situation the axons are from points in the retina that are far enough apart for normal wave statistics to result in maximum competition (Fig. 4, red). The target cell must then choose between one of the two temporally distinct input bursts. This results in a subset of normal and ectopic RFs, since either group can out-compete the other (Fig. 4, red). The existence of split/dual receptive fields suggests that this competition window does not last indefinitely, and under some conditions inputs from disparate regions of the retina can coexist on one collicular neuron. RGCs that are sufficiently far apart spatially have temporal gaps between their bursts that are large enough to prevent competition with each other. In this situation, the collicular cell, not being able to strengthen or weaken either group, ends up with a RF that has multiple peaks (Fig. 4, light blue). Enlarged or patchy receptive fields (Fig. 4, tan), may be due to innervation by several patches of non-competing regions of the retina that appear as one RF due to inherent limits in our ability to resolve details of the RFs. It is also possible that a SC cell receives inputs from several regions of the retina, so that no one region has enough neighbouring (coactive) axons to mutually reinforce each other, so that all inputs remain, perhaps in an immature state, reminiscent of the $\beta2^{-/-}$ (retinal wave mutant) mouse phenotype (Shah & Crair, 2008). The effect of receiving unbiased input from several non-coactive regions of the retina may replicate the de-correlation of activity seen in $\beta2^{-/-}$ mice. The difference here is that the lack of coordinated firing arises from the spatially dispersed nature of the input rather than a lack of temporally patterned retinal activity. This suggests that retinal input needs to drive collicular cell activity strongly in order to evoke activity-dependent changes in synaptic strength. It also suggests that bursting from single inputs in the absence of correlated activity is not sufficient to refine the map.

Implications of the altered receptive fields in BMPR mutants for a burst timing-dependent learning rule

In the BMPR mutants, topographic instruction supplied by molecular factors is disrupted, leading to the altered pattern of projections of dorsal RGC axons to ventral targets in the SC. However, because the mutation is targeted specifically to the retina and produces changes in retinal ganglion cell fate, activity-dependent homeostatic mechanisms and synaptic plasticity, such as long-term potentiation and depression, are probably intact in the SC. RGCs fire action potentials in bursts during development as the result of spontaneous waves of activity that sweep across the retina (Wong *et al.* 1993; Wong, 1999). Synapses between RGCs and lateral geniculate nucleus (LGN) neurons exhibit a burst timing-dependent plasticity (BTDP) learning rule (Butts *et al.* 2007). A similar learning rule may act between RGCs and SC neurons (Shah & Crair, 2008) and refine the connectivity to reflect the statistics of the input pattern of RGC firing. Since the pattern of connectivity between the retina and the SC governs the form and location of the aberrant SC neuron RFs, the characteristic features of RFs observed in the BMPR mutants allow us to make specific predictions about the shape of the BTDP. Cells bursting at the same

are the locations of two electrode penetrations yielding corresponding receptive fields that overlap in visual space (contoured red and yellow RFs overlap; right). Indicated by yellow and red discs (right) are the response regions in visual space predicted for control neurons. Indicated as a blue X (left) is the location in a control SC that has a RF centred at the location where the 2 ectopic RFs are. This result illustrates the physiological manifestation of an anatomical ectopic spot in the BMPR mutant, with two different regions in the retina projecting to the same ectopic region in the SC.

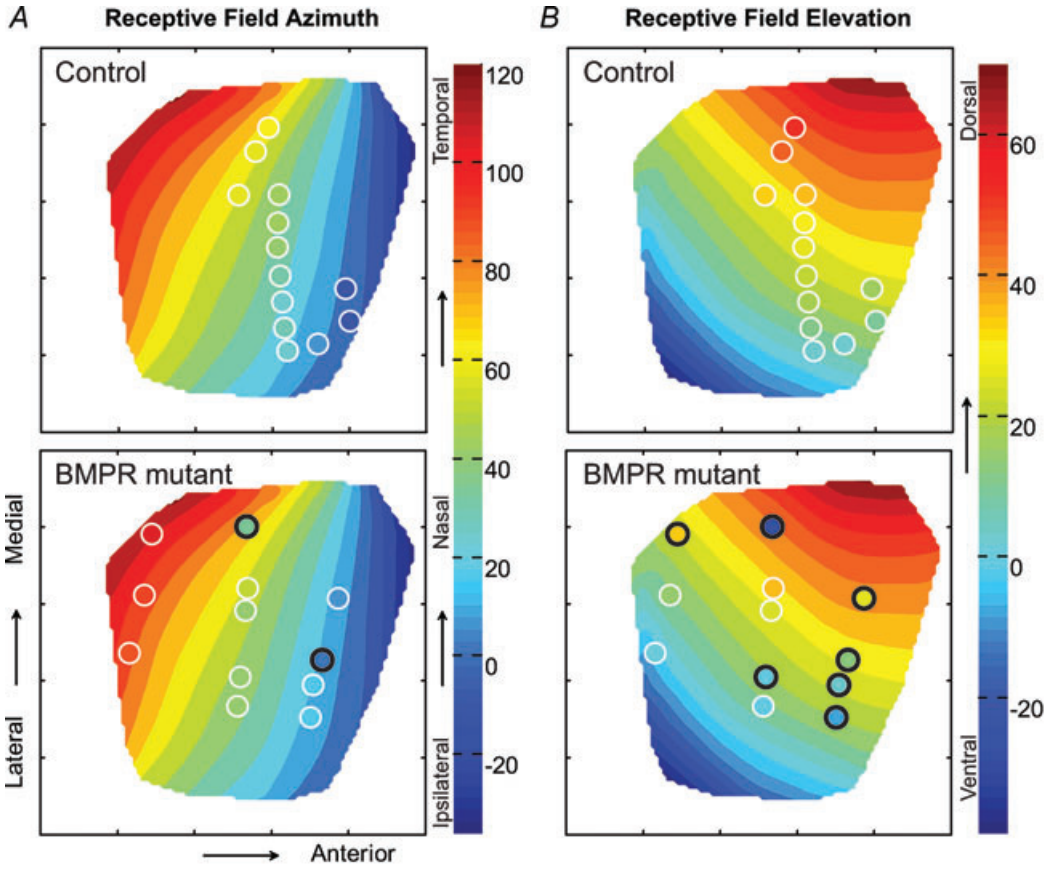

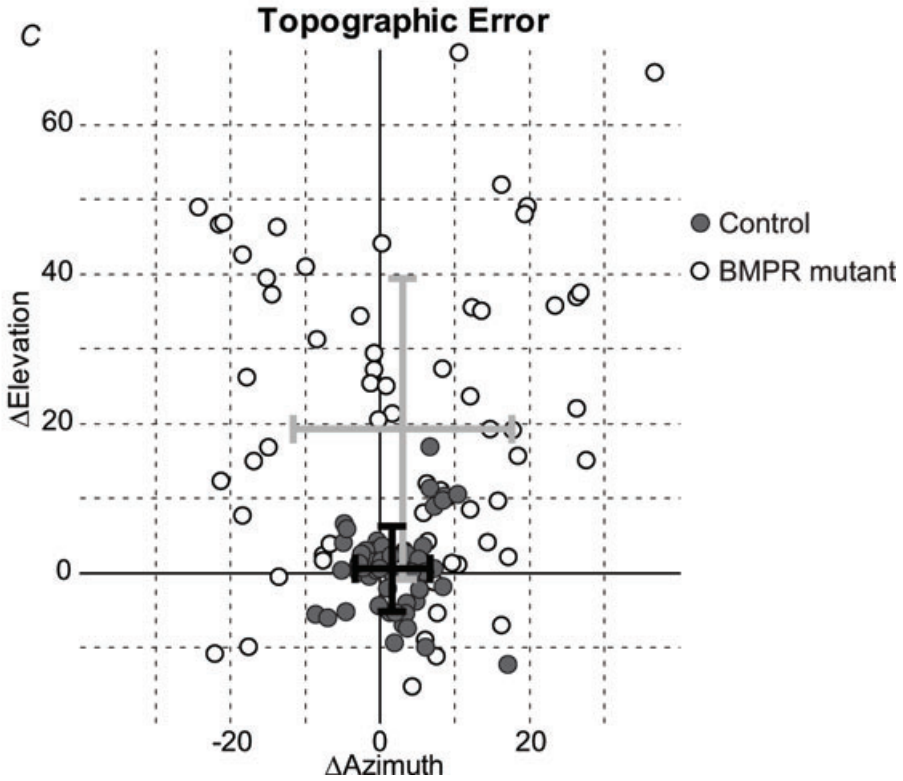

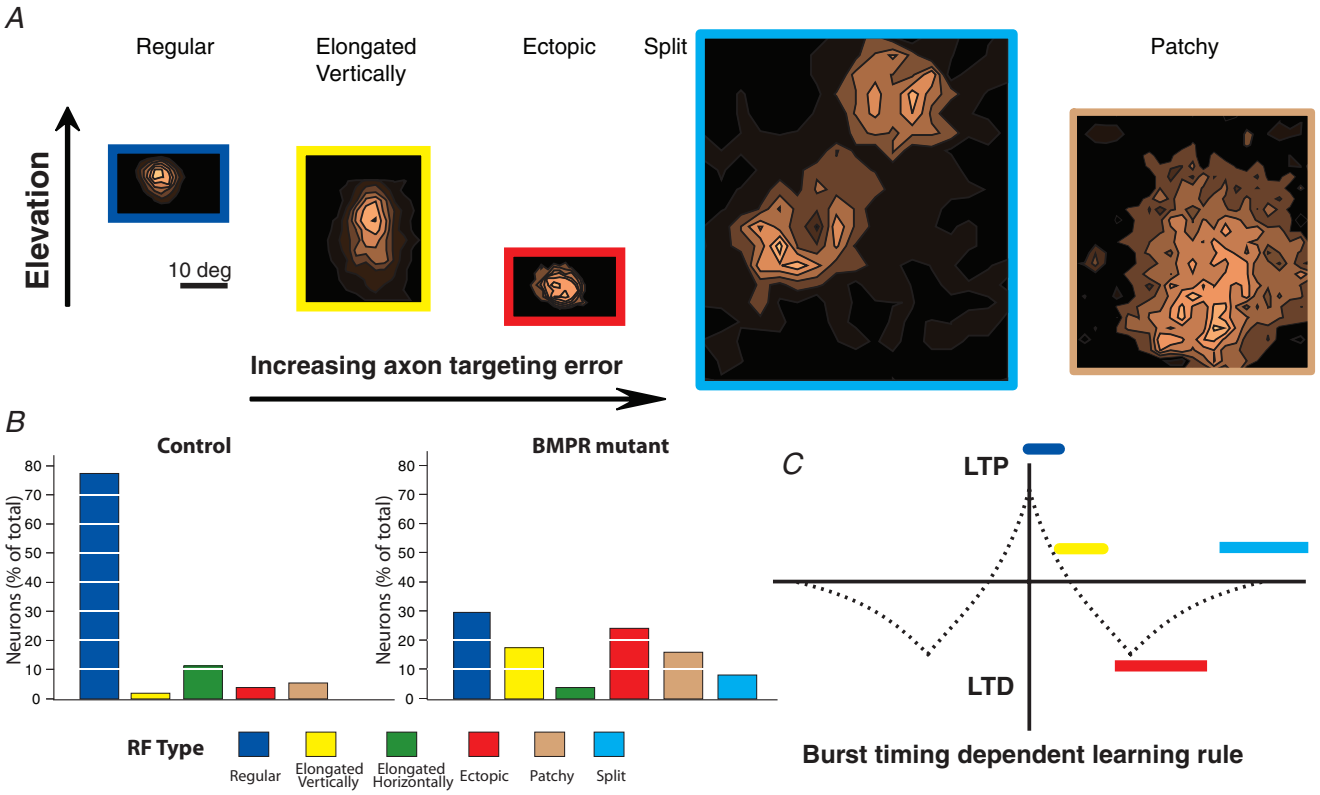

Figure 4. Receptive field properties of BMPR mutants predict the nature of activity-dependent learning rules
A, examples of RFs obtained in the BMPR mutant mice, showing regular (dark blue outline), elongated vertically (yellow), ectopic (red), split (light blue) and patchy (tan) receptive fields. *B*, RF types and their relative occurrence in control (left) and BMPR mutant (right) mice. Regular RFs are by far the most common in control mice (left), and only infrequently are vertically elongated, ectopic, patchy or split RFs encountered. In contrast, irregular receptive fields are frequently encountered in BMPR mutant mice (right). *C*, the predicted learning rule; normal RFs (dark blue) are an outcome of coactive inputs cooperating to strengthen each other at the expense of other afferents. Elongated RFs (yellow) result from minor topographic errors that are not corrected by the learning rule because the inputs arrive from regions of the retina that have a temporal difference in the learning rule that does not strengthen or weaken inputs. When inputs are sufficiently separated spatially in the retina, their temporal code falls under the region of the learning rule that causes competition between inputs (red). This results in a mixture of regular and ectopic RFs. For inputs whose burst timing falls beyond the region of competition (light blue), the learning rule does not allow the strengthening or weakening of either source of inputs, resulting in split/dual receptive fields. A special case of enlarged receptive fields arises when the inputs are scattered from across the region, recreating the phenotype observed in mice lacking retinal waves. Uncorrelated activity caused by axon dispersion, rather than the lack of retinal waves results in the same effect.

Figure 3. BMPR mutants display numerous topographically displaced RFs
A, panels show interpolations of the variation in RF location for horizontal (azimuth) visual space as a function of electrode location in a normalized SC map. *B*, similar interpolations in vertical (elevation) visual space. The RF locations of an example control mouse (top of *A* and *B*) overlay the Drager map. Each electrode location is indicated with a circle and the colour inside indicates the location of the RF's centre in the corresponding axis of visual space. Each control RF qualitatively matches the predicted RF location from the Drager map in both horizontal (left top) and vertical (right top) visual space. The example BMPR mutant mouse (bottom) has examples of numerous ectopic RFs. Ectopic RF locations in azimuth are fewer for this example (bottom left; black circles) compared to the number of RFs ectopic in elevation (bottom right; black circles). Ectopic RFs are defined as having centres with $>$ 15 deg variation from that predicted for the corresponding electrode location in the Drager map. *C*, scatter plot of topographic error in control (filled grey circles) mice and BMPR mutant (open circles) mice. While the deviation of control RFs from the Drager map is small (standard deviation; black error bars) and close to zero, mutant RFs have a significantly higher mean vertical error (light grey error bars, $P \ll 0.01$), indicative of the ventralization of dorsal retinal axons. While there is a large amount of scatter in the BMPR mutant RF locations along the azimuth (Levene test: $P \ll 0.01$), they do not display any bias (difference in mean values) towards either nasal or temporal directions (*t* test: $P = 0.5$).

or similar times would create correlated activity in postsynaptic targets leading to the central potentiation window in the BTDP rule (Fig. 4*C*, dark blue). If the distribution of inputs to a region of the SC is skewed by targeting errors, the resultant RF will not develop a symmetric shape as these inputs will neither compete nor reinforce each other, as their activity would be offset in time (Fig. 4*C* yellow). As the separation between RGC inputs increases spatially, further decreases in the temporal overlap of their bursts will force them to compete for synaptic contacts onto SC cells resulting in a distribution of normal and ectopic RFs (Fig. 4*C*, red). Butts *et al.* (2007) observed a BTDP rule in the LGN that is symmetrical with a central potentiation peak for coincident bursts and a depression phase for non-coincident bursts that is extremely broad. With a very broad depression window, two disparate locations in the retina could not synapse onto the same cell, as they would always be in competition. While such a broad learning rule might exist in the LGN, our observation of split RFs (6/74) in the SC of BMPR mutants that are spaced 40.5 ± 2.2 deg apart, suggests that distant locations on the retina are able to innervate the same neuron in the SC. This places a hard limit on the width of the BTDP window that can affect the state of a synapse (Fig. 4*C*, cyan), which we estimate to be about 1 s based on the size of the mouse eye and the properties of retinal waves (Bansal *et al.* 2000; Schmucker *et al.* 2004; Demas *et al.* 2006).

Homeostasis and RF properties in BMPR mutants

In control animals, neurons with large RFs have small peak responses, and vice versa (Fig. 1 and Chandrasekaran *et al.* 2007), a property we have termed 'response homeostasis'. In the BMPR mutants, response homeostasis is maintained, despite the huge variance in RF sizes. The maintenance of response homeostasis in the BMPR mutants in neurons with ectopic, enlarged or even split RFs, suggests that response homeostasis is regulated by a mechanism in SC neurons that is distinct from the control of RGC axon guidance. The apparent requirement for cooperation before any particular group of axons can take over a SC cell suggests that the inputs 'chosen' by a postsynaptic cell strongly depends on the initial pattern of retinal input. If the initial patterning does not have any bias (and therefore no cooperation), the SC neuron simply abstains from choosing. This is similar to the maintenance of response homeostasis in $\beta 2^{-/-}$ mice (Chandrasekaran *et al.* 2007), but unlike the situation in Adenylyl Cyclase 1 mutant mice, which are thought to have intact axon guidance but defects in synapse formation and response homeostasis in the superior colliculus (R. D. Shah, O. S. Dhande, A. R. Chandrasekaran, A. Anishchenko, J. Elstrott, T. Iwasato, E. Swindell, M. Jamrich, S. Itohara, M. B. Feller & M. C. Crair, unpublished observations).

Our results from the analysis of BMPR mutant mice receptive fields strongly suggest that molecular guidance factors play a key role in setting up a template upon which activity-dependent factors then subsequently act. They also show that retinal waves cannot correct for large global defects in targeting, and they place several restrictive predictions on the nature of the synaptic learning rules that govern activity-dependent refinement of retinotopic maps and the emergence of receptive fields.

References

Bansal A, Singer JH, Hwang BJ, Xu W, Beaudet A & Feller MB (2000). Mice lacking specific nicotinic acetylcholine receptor subunits exhibit dramatically altered spontaneous activity patterns and reveal a limited role for retinal waves in forming ON and OFF circuits in the inner retina. *J Neurosci* **20**, 7672–7681.

Bartlett JE, Lee SM, Mishina Y, Behringer RR, Yang N, Wolf J, Temelcos C & Hutson JM (2002). Gubernacular development in Müllerian inhibiting substance receptor-deficient mice. *BJU Int* **89**, 113–118.

Brainard DH (1997). The psychophysics toolbox. *Spat Vis* **10**, 433–436.

Butts DA, Kanold PO & Shatz CJ (2007). A burst-based "Hebbian" learning rule at retinogeniculate synapses links retinal waves to activity-dependent refinement. *PLoS Biol* **5**, e61.

Butts DA & Rokhsar DS (2001). The information content of spontaneous retinal waves. *J Neurosci* **21**, 961–973.

Cang J, Niell CM, Liu X, Pfeiffenberger C, Feldheim DA & Stryker MP (2008). Selective disruption of one Cartesian axis of cortical maps and receptive fields by deficiency in ephrin-As and structured activity. *Neuron* **57**, 511–523.

Chandrasekaran AR, Plas DT, Gonzalez E & Crair MC (2005). Evidence for an instructive role of retinal activity in retinotopic map refinement in the superior colliculus of the mouse. *J Neurosci* **25**, 6929–6938.

Chandrasekaran AR, Shah RD & Crair MC (2007). Developmental homeostasis of mouse retinocollicular synapses. *J Neurosci* **27**, 1746–1755.

Demas J, Sagdullaev BT, Green E, Jaubert-Miazza L, McCall MA, Gregg RG, Wong RO & Guido W (2006). Failure to maintain eye-specific segregation in nob, a mutant with abnormally patterned retinal activity. *Neuron* **50**, 247–259.

Drager UC & Hubel DH (1976). Topography of visual and somatosensory projections to mouse superior colliculus. *J Neurophysiol* **39**, 91–101.

Furuta Y, Lagutin O, Hogan BL & Oliver GC (2000). Retina- and ventral forebrain-specific Cre recombinase activity in transgenic mice. *Genesis* **26**, 130–132.

Hebb DO (1949). *The Organization of Behavior*. John Wiley & Sons, New York.

Himanen JP, Chumley MJ, Lackmann M, Li C, Barton WA, Jeffrey PD, Vearing C, Geleick D, Feldheim DA, Boyd AW, Henkemeyer M & Nikolov DB (2004). Repelling class discrimination: ephrin-A5 binds to and activates EphB2 receptor signaling. *Nat Neurosci* **7**, 501–509.

McLaughlin T & O'Leary DD (2005). Molecular gradients and development of retinotopic maps. *Annu Rev Neurosci* **28**, 327–355.

Mishina Y, Hanks MC, Miura S, Tallquist MD & Behringer RR (2002). Generation of Bmpr/Alk3 conditional knockout mice. *Genesis* **32**, 69–72.

Mishina Y, Suzuki A, Gilbert DJ, Copeland NG, Jenkins NA, Ueno N & Behringer RR (1995). Genomic organization and chromosomal location of the mouse type I BMP-2/4 receptor. *Biochem Biophys Res Commun* **206**, 310–317.

Murali D, Yoshikawa S, Corrigan RR, Plas DJ, Crair MC, Oliver G, Lyons KM, Mishina Y & Furuta Y (2005). Distinct developmental programs require different levels of Bmp signaling during mouse retinal development. *Development* **132**, 913–923.

O'Leary DD & McLaughlin T (2005). Mechanisms of retinotopic map development: Ephs, ephrins, and spontaneous correlated retinal activity. *Prog Brain Res* **147**, 43–65.

Pelli DG (1997). The VideoToolbox software for visual psychophysics: transforming numbers into movies. *Spat Vis* **10**, 437–442.

Plas DT, Dhande O, Lopez JE, Murali D, Thaller C, Henkemeyer M, Furuta Y, Overbeek P & Crair MC (2008). Bone morphogenetic proteins, eye patterning and retinocollicular map formation in the mouse. *J Neurosci* **28**, 7057–7067.

Schmucker C & Schaeffel F (2004). A paraxial schematic eye model for the growing C57BL/6 mouse. *Vis Res* **44**, 1857–1867.

Shah RD & Crair MC (2008). Retinocollicular synapse maturation and plasticity are regulated by correlated retinal waves. *J Neurosci* **28**, 292–303.

Tavazoie SF & Reid RC (2000). Diverse receptive fields in the lateral geniculate nucleus during thalamocortical development. *Nat Neurosci* **3**, 608–616.

Torborg CL & Feller MB (2005). Spontaneous patterned retinal activity and the refinement of retinal projections. *Prog Neurobiol* **76**, 213–235.

Wong RO (1999). Retinal waves and visual system development. *Annu Rev Neurosci* **22**, 29–47.

Wong RO, Meister M & Shatz CJ (1993). Transient period of correlated bursting activity during development of the mammalian retina. *Neuron* **11**, 923–938.

Yi SE, Daluiski A, Pederson R, Rosen V & Lyons KM (2000). The type I BMP receptor BMPRIB is required for chondrogenesis in the mouse limb. *Development* **127**, 621–630.

Acknowledgements

We gratefully acknowledge members of the Crair lab for insightful discussions and helpful comments on the manuscript. This work was supported by NIH grants R01 MH062639, R01 EY015788, P30 EY000785.